12 Physics performance

12.1 Introduction

The Transition Radiation Detector (TRD) was added in the central barrel of the ALICE experiment [1] to identify electrons and positrons in the central rapidity region primarily in central Pb–Pb collisions at the full LHC energy of 5.5 TeV /nucleon pair [2]. The physics motivation is the measurement of heavy-vector resonances, J/ψ and Υ families in the dielectron channel and of open charm and open beauty, i.e. the D and B mesons, via their semi-leptonic decays. Furthermore, coincidences of electrons in the central barrel with muons in the forward muon arm are expected to provide information on the production of D and B mesons at the rapidity interval $1 < y < 3$, intermediate between that of the central barrel and the dimuon arm. With the TRD providing a L1 trigger on high p_{t} charged particles the measurement of high E_{t} jets might be possible in the central barrel. The contribution of such measurements to the understanding of the phase transition and the properties of the deconfined phase is detailed in the TRD TP [2], in Ref. [3] and references therein.

This chapter focuses on central Pb–Pb collisions that present the major challenge for a dedicated heavy-ion experiment. Emphasis is placed on acceptances of the TRD for measurement of quarkonia and open charm and open beauty. We also provide information on resolution and background sources.

12.2 Primary collision

There are large uncertainties in the theoretical predictions of the particle multiplicities and their spectral distributions produced in central Pb–Pb collisions at LHC energies. Hence the uncertainties of the input distributions used in the simulations presented here dominate by far the statistical and systematical errors of the presented results.

The strategy in ALICE has been to perform all the TDR studies for the detector optimization assuming the highest anticipated charged particle rapidity density $\mathrm{d}N_{\mathrm{ch}}/\mathrm{d}y = 8000$ at mid-rapidity, for central Pb–Pb collisions, in accordance with the one used for the ALICE TP [1]. The predictions at the time, summarized in Ref. [4] vary in the range of 1600 to 8000.

The rapidity density of $\mathrm{d}N_{\mathrm{ch}}/\mathrm{d}y = 8000$ results in $\approx$ 20 000 charged particles entering the TRD. However, there is increasing evidence that such extreme multiplicity densities might not be reached. Recent data from the Relativistic Heavy Ion Collider (RHIC) on central Au–Au collisions including this summer's measurements at $\sqrt{s} = 200$ GeV provide today first constraints on the theoretical models. Within a high density QCD model Kharzeev and Levin [5] have recently derived an analytical scaling function for the multiplicity density as a function of $\sqrt{s}$. We have used their model to fit the results of the charged particle density for Au–Au at $\sqrt{s} = 56$, $\sqrt{s} = 130$ and $\sqrt{s} = 200$ GeV measured by the PHOBOS Collaboration [6]. The extrapolation to LHC energy, a factor of $\sim$ 27 higher, gives an estimate of $\mathrm{d}N_{\mathrm{ch}}/\mathrm{d}y = 1700$. The errors in the measurement are still large and give a maximum of $\mathrm{d}N_{\mathrm{ch}}/\mathrm{d}y = 2600$ and a minimum of $\mathrm{d}N_{\mathrm{ch}}/\mathrm{d}y = 1100$. Further evidence supporting the expectation of lower multiplicities is provided by the calculation of Eskola et. al. [7] of the $\sqrt{s}$ dependence of the charged particle density in terms of a perturbative QCD model including parton saturation. Their results are shown in Fig 12.1 and predict a $\mathrm{d}N_{\mathrm{ch}}/\mathrm{d}\eta$ = 2300 at LHC energies.

Considering the uncertaintly in extrapolation from RHIC to LHC energy as well as the systematic uncertainty in the models for particle production the prudent strategy adopted by ALICE for all other detectors, was also followed in the present TDR.

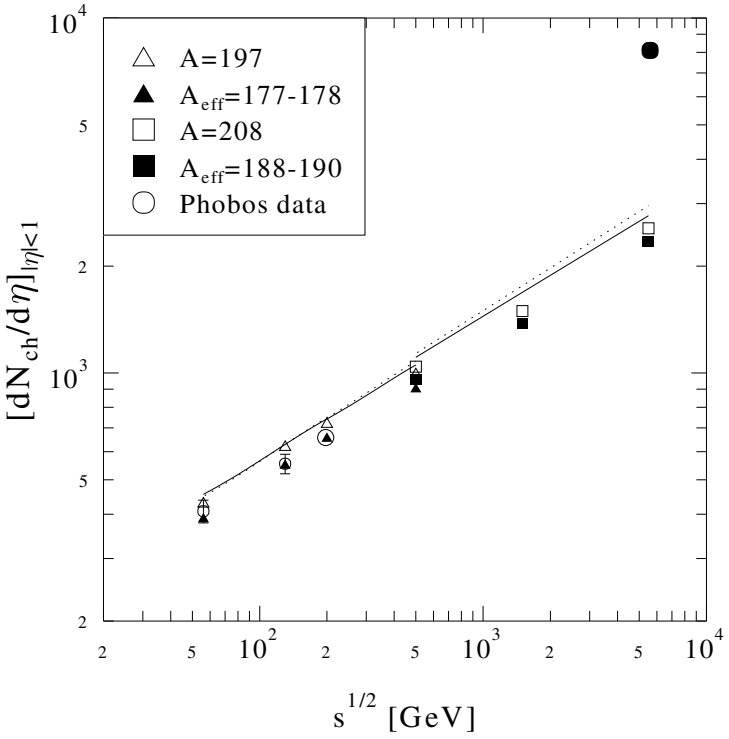

Figure 12.1: Midrapidity charged particle densities calculated in a perturbative QCD model by Eskola et. al. as function of $\sqrt{s}$. The full dot corresponds to the worst case scenario used in the present simulations.

The shape of the transverse momentum spectra of produced particles is also not known for LHC energy. For the simulation of pions to evaluate the performance of the TRD the shape of the p_t spectra was parametrized by a power law fitted to the CDF data [8] in agreement with the shape predicted by the HIJING [9] model. For kaons a p_t scaling from the pion distribution has been used. However, the pion spectra measured in central Au–Au collisions by the PHENIX collaboration [10] are considerably steeper than those of pp and the HIJING model, see Fig. 12.2. Spectra in Pb–Pb collisions at LHC energies that are softer than currently assumed, would result in a much smaller pion yield at high p_t.

Thus, the recent RHIC data indicate that both the charged particle density at mid-rapidity and the shape of the pion p_t spectra assumed in the present simulation and upon which depends the background in the TRD detector, represent the worst case scenario and might already provide a large safety factor.

The yields of J/ψ and ϒ, also unknown in such collisions, were estimated extrapolating from existing pp data in the framework of the colour evaporation model and scaling up to central Pb–Pb collisions, as described in the CMS note [11], see also Section 6.5. According to this extrapolation 0.5 J/ψ and 0.012 ϒ per event are expected.

The yields of D and B mesons in central Pb–Pb collisions are expected to be large. To estimate them [12] a reasonable baseline for the production of $c\bar{c}$ and $b\bar{b}$ in pp collisions at $\sqrt{s} = 5.5$ TeV had to be obtained first. For this, PYTHIA [13] was used to calculate in leading order $\sigma(c\bar{c})$ and $\sigma(b\bar{b})$ using the MRST [14], CTEQ5M1 [15] and GRV(98)HO [16] set of parton density functions including the ESK98 [17] parametrisation of nuclear shadowing effects. A K factor of 2 was used to estimate the next to leading order corrections. The yields were then scaled up from pp to central Pb–Pb using the average number of collisions from a Glauber calculation. The average of these calculations give $dN(c\bar{c})/dy = 115$ and $dN(b\bar{b})/dy = 4.6$. PYTHIA was then used to calculate the hadronization, resulting in a total multiplicity per event of 230 D mesons: 140 D^0 and $\overline{D}^0$, 45 $D^{\pm}$, 27 $\overline{D}_s^0$ and 9 B mesons: 3.7 B_d^0 and $\overline{B}_d^0$, 3.6 $B^{\pm}$ and 1.1 B_s^0.

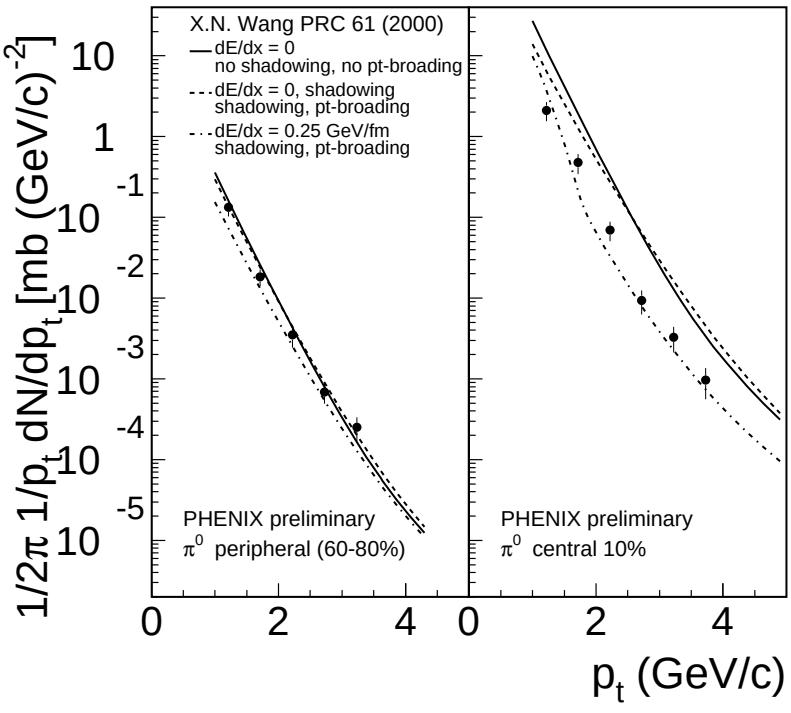

Figure 12.2: Transverse momentum spectra measured by PHENIX for Au–Au collisions at $\sqrt{s} = 130$ GeV compared to the HIJING predictions.

In Ref. [2], the signal/background ratio R_s for the detection of J/ψ and Υ mesons was evaluated for $dN_{ch}/dy = 8000$ and using cross sections and transverse momentum distributions as discussed above. It lead to $R_s > 1$ for Υ and $R_s > 0.1$ for J/ψ. Since global tracking through the whole ALICE apparatus is not yet available, we will not provide new estimates of R_s here. We note, however, that with charged particle multiplicities and p_t spectral shapes as extrapolated from recent RHIC data the R_s values might increase substantially, perhaps by an order of magnitude.

12.3 Simulation environment

AliRoot [18], the object-oriented framework developed in ALICE, version V3.05, was used for the generation, detector response simulation and analysis of the simulated data as described in Chapter 11. The framework provides a seamless interface to GEANT3 [19], GEANT4 [20] and soon to FLUKA [21] for particle transport. It provides the flexibility to use GEANT3 or GEANT4 with the same definition of detector geometry. FLUKA is used standalone for radiation background studies, with a less detailed description of the geometry of the layout which is described using the ALIFE module [22]. Recently FLUKA was extended with the implementation of thermal neutron capture in Xenon for the TRD background calculations [23].

In AliRoot there are different modules for the generation of the input particles as well as for the simulation of the detector response for each detector. The geometry of the detectors is described in detail while for the detector response a ‘detailed’ and a ‘fast’ mode have been implemented. The reconstruction strategies and algorithms for the different detectors as well as for the global tracking in the central barrel are currently being actively developed aiming at a ‘physics run’ for the ALICE Physics Performance Report.

12.3.1 Simulation of the detector layout

The detection of di-leptonic decays of heavy quarkonia and semi-leptonic decays of B and D mesons require the measurement of high p_t electrons; therefore this study was performed assuming a 0.4 T magnetic field, which the L3 magnet can provide according to current evaluations and tests [24]. The production vertex of the primary particles was fixed at the center of the experiment. The full configuration of the TRD detector was used as is implemented in AliRoot and described in Chapter 11. A picture of the TRD layout is shown in Colour Fig. 3. The TRD detector is embedded in the space frame as shown in Fig. 2.1. The space frame geometry is always included in the simulation when the TRD is activated.

In the 'detailed' TRD simulation mode, charged particles losing energy in the chamber gas produce primary and secondary electrons from ionization as described in Chapter 11. Each electron produces a 'hit' from which the digitized signal for every pad is derived. That way detailed studies of the chamber performance can be carried out. However, for some purposes this is a too detailed and slow procedure. Therefore, a 'fast' simulation mode for the detector response was also implemented; charged particles that cross the active area of one of the multiwire proportional chambers produce one hit only which is placed in the center of the active part of the chamber. Hence particles traversing all 6 planes of the TRD through their active area produce a total of 6 hits.

12.3.2 Simulation of input particles

Different type of event generators, provided in AliRoot, were used to generate the different type of input particles depending on the performed study:

- the 'signal'-generating particles were produced according to a parametrization of their y and p_t distributions
- the bulk of produced particles in a Pb–Pb collision, pions and kaons, were generated using the so called 'parametrized HIJING' event generator, using their parametrized y and p_t distributions as well as their relative yields, normalized to a total number of charged particles of 8000 in the region $-0.5 < \eta < 0.5$.

The 'signal'-generating particles Υ, J/ψ, as well as B and D mesons, were produced with flat rapidity and p_t distributions and then were weighted with a realistic p_t distribution [2]:

$$\frac{dn}{dp_t} = \frac{p_t}{[1+(\frac{p_t}{p_t^\circ})^2]^n} \tag{12.1}$$

with the parameters p_t° and n as given in Table 12.1 for the different particles.

Table 12.1: Parameters of the functional form used to describe the p_t distribution of different particles.

particle	p_t°	n
Υ	4.7	3.5
J/ψ	3.5	2.3
B	4.0	3.6
D	4.08	9.4

Υ mesons were generated in the rapidity interval $-1.2 < y < 1.2$ and $p_t < 10$ GeV/c , J/ψ in $-1.5 < y < 1.5$ and $p_t < 10$ GeV/c , B and D mesons in the interval $-5 < y < 5$ and $p_t < 10$ GeV/c . PYTHIA was

used to force the decay of the primary particles: ϒ and J/ψ exclusively into di-electrons, B and D mesons exclusively into the semi-leptonic channels. The rapidity interval was chosen such that primary particles outside this interval do not emit their decay products into the TRD acceptance. Those distributions were used to evaluate the TRD acceptance and the effect of the L1 trigger.

The 'parametrized HIJING' event generator was used to generate pions and kaons of central Pb–Pb collision for background estimates.

12.3.3 Simulation studies

For the evaluation of the acceptances only the TRD detector and the space frame were included in the simulation of the ALICE set-up. For the transport of all generated particles through the TRD layout only decays, energy loss and multiple scattering were enabled from all physics processes implemented in GEANT3. In this way all primary electrons could be accounted for until they exited the TRD and there was no other source of background electrons. The 'fast' detector response simulation option was used. The acceptance for any of the parent particles was defined by the requirement that its daughter particles have to traverse at least 5 planes of the TRD through their active area, i.e. to produce at least 5 hits in total. Optimization of the reconstruction algorithms using the data produced by the 'detailed' simulation has shown that this would insure a good track reconstruction and particle identification probability. The L1 TRD trigger, as described in Chapter 6, is designed to select charged particles with $p_t > 3$ GeV/c traversing the TRD detector. A ϒ or J/ψ trigger requires a pair of opposite charged electrons with p_t above this threshold.

For the reconstruction of the invariant mass and the estimate of the background due to primary and secondary particles, as well as γ conversions, all detectors in the central barrel were included in the simulation and all physics processes in GEANT3 were activated.

12.4 ϒ and J/ψ mesons

12.4.1 Acceptance

To evaluate the ϒ and J/ψ acceptance 900 000 primary particles of each kind were generated with flat rapidity and p_t distributions in the interval $-1.2 < y < 1.2$ ($-1.5 < y < 1.5$ for J/ψ) and $p_t < 10$ GeV/c , all decaying into e^+e^- pairs. The acceptance and the effect of the L1 trigger was then evaluated using the p_t-weighted distributions of the parent particles. The p_t-weights were generated using eq. 12.1 and the corresponding parameters given in Table 12.1.

Figures 12.3 and 12.4 show, on the top row, the rapidity and p_t distributions of the parent particles and, on the lower row, those of their decay electrons. The full curve in each figure corresponds to the input distribution. The dashed curves show the distributions of particles in the TRD acceptance with the condition that both decay particles cross at least 5 chambers. The main condition for a L1 trigger is a p_t cut of, e.g., 3 GeV/c for each particle (see Chapter 6). The dotted histogram shows the effect of the L1 trigger: the distributions are plotted with an additional requirement of $p_t > 3$ GeV/c for both decay particles. The rapidity distribution of the accepted ϒ covers the range $|y| < 1.0$ and is Gaussian-like with a $\sigma = 0.39$; that for J/ψ has the same coverage and is somewhat flatter with a $\sigma = 0.41$.

The ϒ and J/ψ acceptances under the trigger requirement are shown differentially in the y-p_t plane in Fig. 12.5 for ϒ and in Fig. 12.6 for J/ψ. In the lego plot of the ϒ acceptance a small dip is clearly seen developing at $p_t \sim 6$ GeV/c . This is due to the fact that low p_t ϒ mesons decay by emitting e^+e^- pairs where both leptons have a p_t above 3 GeV/c and hence pass the trigger condition. The decay of intermediate p_t ϒ mesons, of $p_t \sim 6$ GeV/c , can be asymmetric in the laboratory frame with one of the decay particles having p_t less than 3 GeV/c ; therefore those ϒ are lost due to the L1 trigger condition. The differential ϒ acceptance at mid-rapidity and $p_t < 1$ GeV/c is 54%, while at $p_t = 6$ GeV/c , is 47%.

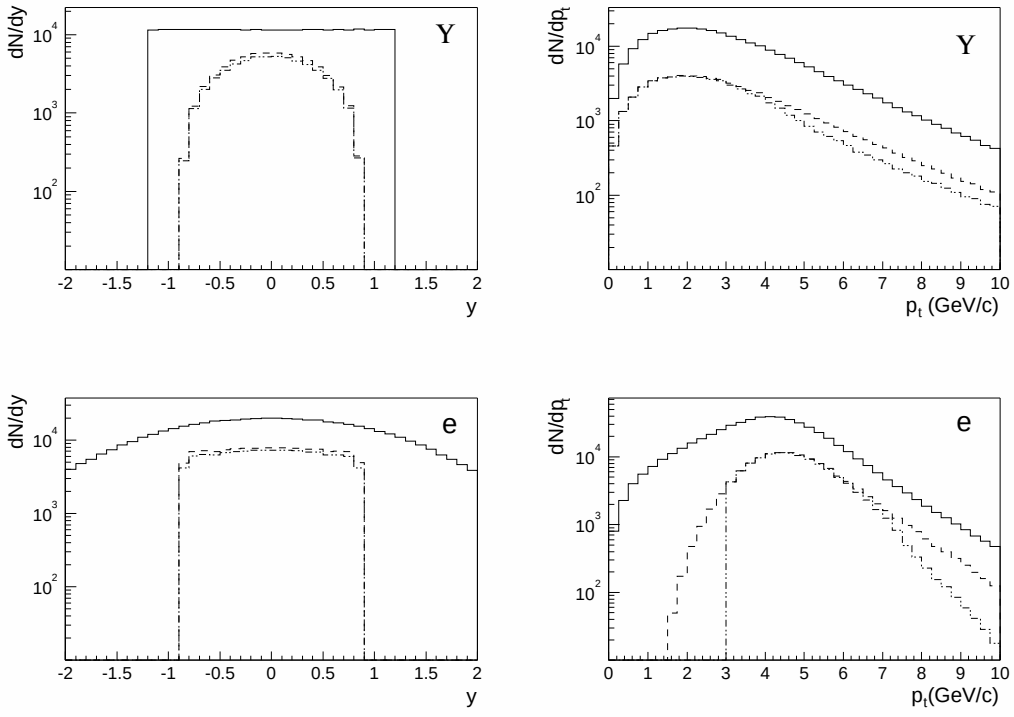

Figure 12.3: Rapidity and p_{t} distributions of Υ and its decay e^+e^-. The solid lines show the input distributions, dashed are those accepted in the TRD and the dotted histograms show the fraction accepted in the TRD with the L1 trigger requirement of $p_{\mathrm{t}} > 3$ GeV/c on the decay particles.

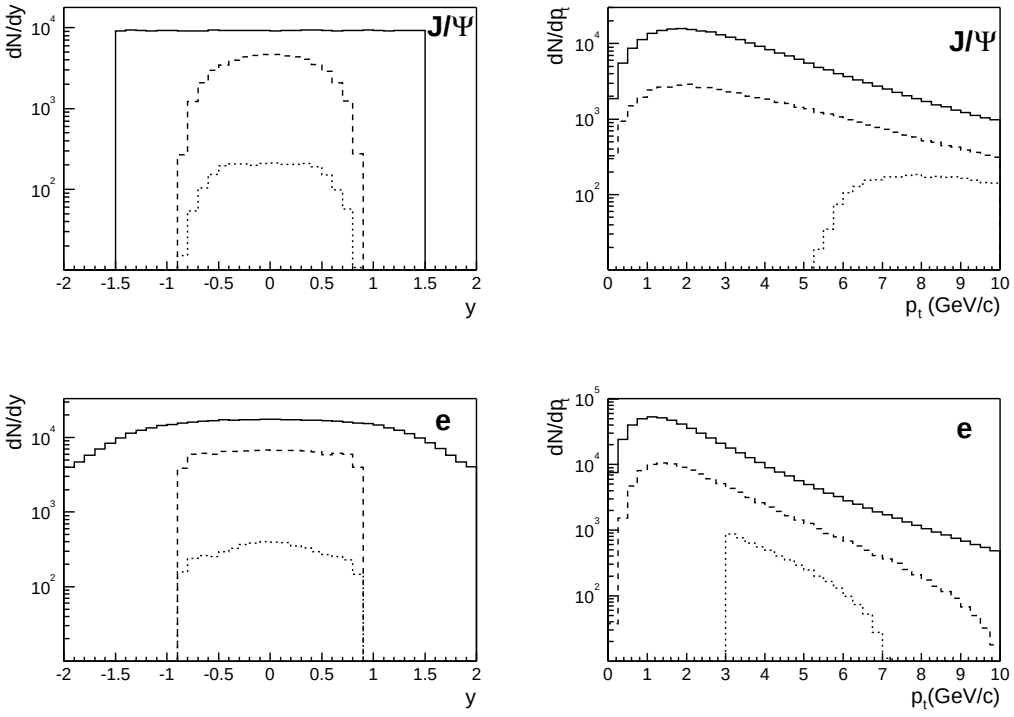

Figure 12.4: Rapidity and p_{t} distributions of J/ψ and its decay e^+e^-.The solid lines show the input distributions, dashed are those accepted in the TRD and the dotted histograms show the fraction accepted in the TRD with the L1 trigger requirement of $p_{\mathrm{t}} > 3$ GeV/c on the decay particles.

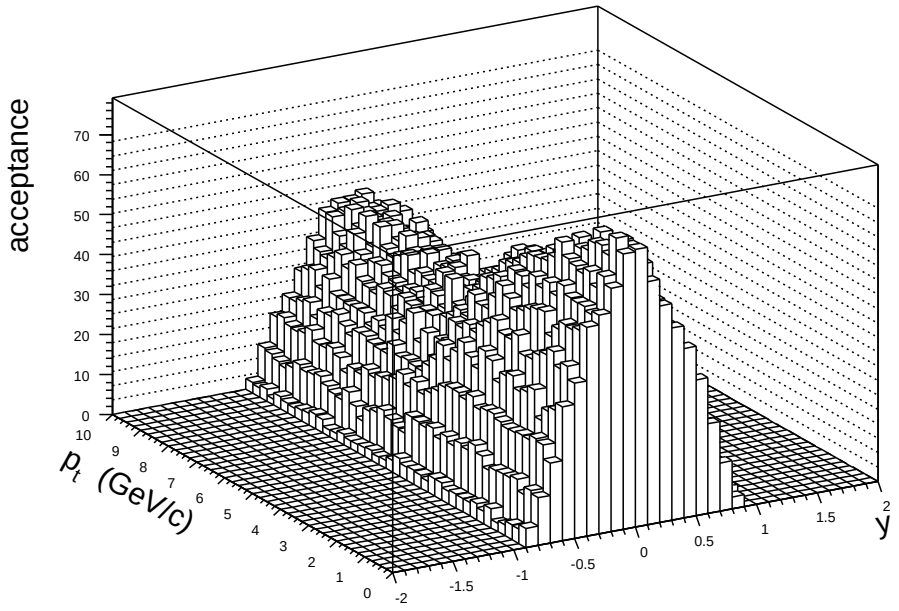

Figure 12.5: Differential y-p_t acceptance in % for the detection of ϒ in the TRD under the L1 trigger condition.

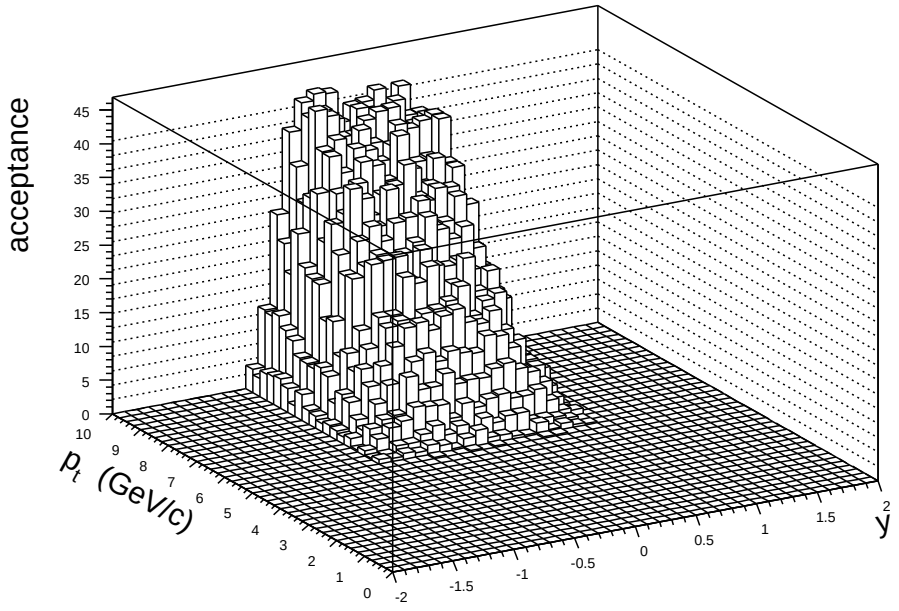

Figure 12.6: Differential y-p_t acceptance in % for the detection of J/ψ the TRD under the L1 trigger condition.

The trigger cut on the p_t of e^+e^- has a much stronger effect on the J/ψ distribution since the mass difference of the J/ψ is much smaller than that of the ϒ; hence the decays of low p_t J/ψ produce e^+e^- pairs that do not make it through the p_t threshold of 3 GeV/c of the trigger. It is only at rather large p_t that the J/ψ decay kinematics allow both of the e^+e^- to have $p_t > 3$ GeV/c . This results in no J/ψ acceptance below a p_t of ~ 5.2 GeV/c under the L1 trigger condition. The differential acceptance at mid-rapidity reaches 37% for a p_t of 10 GeV/c .

The geometrical acceptances for ϒ and J/ψ integrated over the rapidity range $-1.0 < y < 1.0$, the region where there is some acceptance, are summarized in Table 12.2. They are tabulated without and with the L1 trigger condition on their decay particles and for different p_t range of the parent particle.

Table 12.2: Geometrical acceptance for the detection of ϒ and J/ψ in the TRD. They are given for different y and p_t ranges of the parent particles, with and without the L1 trigger p_t cut on the e^+e^- pair.

parent particle	p_t of e^+e^-	y and p_t of parent	TRD accept. (%)
ϒ	no cut	$\|y\| < 1.0$, all p_t	26.6
ϒ	no cut	$\|y\| < 0.5$, $p_t < 3$ GeV/c	42.4
ϒ	$p_t > 3$ GeV/c	$\|y\| < 1.0$, all p_t	24.0
ϒ	$p_t > 3$ GeV/c	$\|y\| < 0.5$, $p_t < 3$ GeV/c	41.7
J/ψ	no cut	$\|y\| < 1.0$, all p_t	29.5
J/ψ	no cut	$\|y\| < 0.5$, $p_t > 6$ GeV/c	62.8
J/ψ	$p_t > 3$ GeV/c	$\|y\| < 1.0$, all p_t	1.4
J/ψ	$p_t > 3$ GeV/c	$\|y\| < 0.5$, $p_t > 6$ GeV/c	16.3

12.4.2 ϒ invariant mass distribution

The best momentum resolution for electrons identified in the TRD will be obtained by combining the information of the TRD, TPC and ITS in a global track fit. Such a procedure using Kalman-filter tracking techniques was implemented in the AliRoot framework and is currently being optimized.

To evaluate the mass resolution with tracking in the TRD only, events containing only ϒ in the rapidity interval $-0.5 < y < 0.5$ and with a realistic p_t distribution given by eq. 12.1 were generated. All the detectors of the central barrel and all physics processes were enabled for the particle transport. The 'detailed' TRD detector response simulation mode was used. The point reconstruction and tracking were performed as described in Section 11.3 and 11.4. From the momentum resolutions obtained with the full off-line tracking the mass resolutions were determined using the same algorithm as was used in the simulations for the TRD trigger (see Chapter 6).

Applying the TRD L1 trigger condition that both e^+e^- have a $p_t > 3$ GeV/c results in an e^+e^- invariant mass distribution shown in Fig. 12.7. The invariant mass distribution is asymmetric with a tail to lower masses due to radiative losses of the electrons in the material before the TRD. The mass resolution for tracking in the TRD only, ignoring the low mass tail resulting from bremsstrahlung losses, has a $\sigma = 245$ MeV/c^2.

The global track fit gives an improved estimator for the original momentum of the e^+e^- pair and, at the same time, will provide a much better momentum resolution. A study was performed using the track reconstruction in the TPC and ITS, but yet without the TRD, to evaluate the mass resolution at the mass of the ϒ as function of the event multiplicity for two magnetic field values. The results, shown in Fig. 12.8, give a mass resolution of about 1% for the full multiplicity and $B = 0.4$ T.

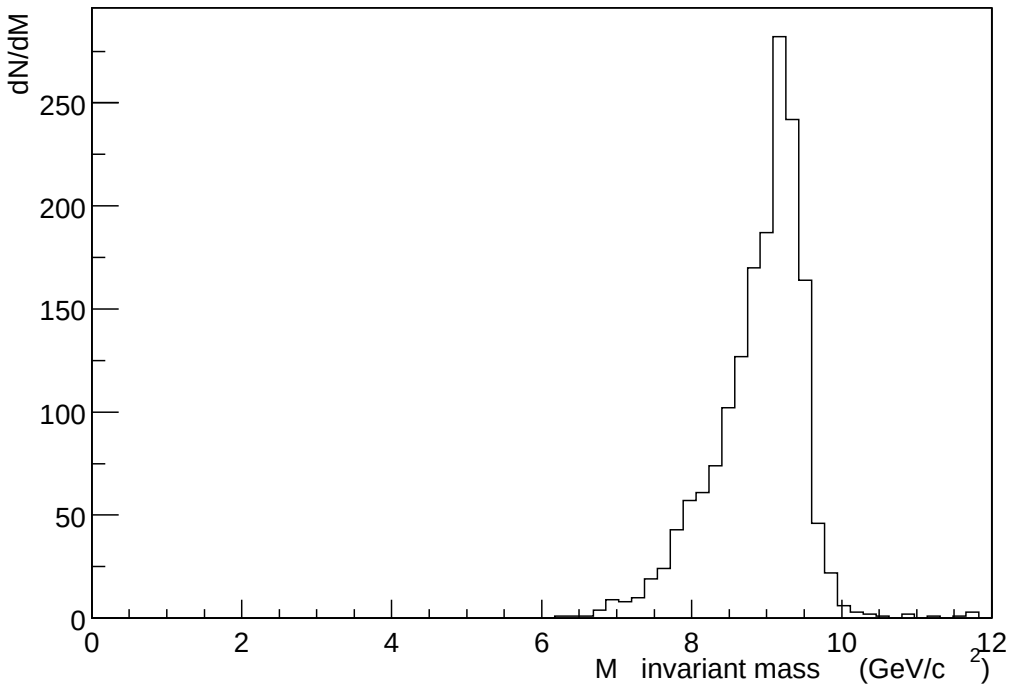

Figure 12.7: Di-electron invariant mass distribution for e^+e^- pairs from ϒ decays as reconstructed in the TRD, including the TRD L1 trigger condition.

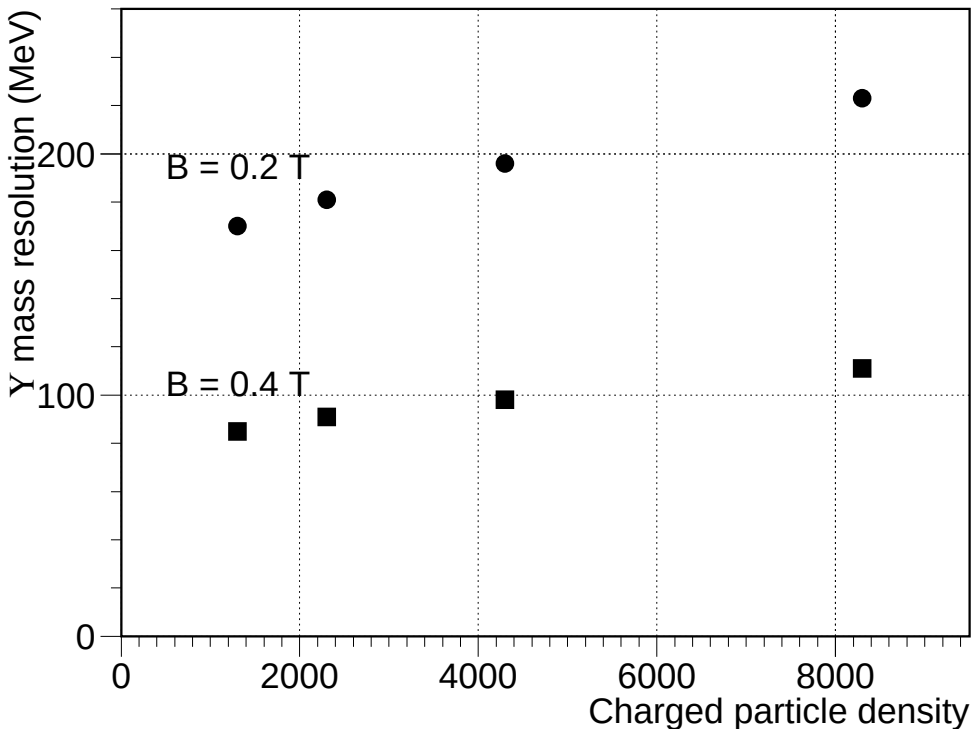

Figure 12.8: Invariant mass resolution for ϒ decaying into e^+e^- as function of the event multiplicity when both tracks are reconstructed in the TPC and ITS.

12.5 B and D mesons

For the calculation of the acceptance for B and D mesons 4 million primary particles, of each kind, were generated with flat distributions in the interval $-5 < y < 5$ and $p_t < 10$ GeV/c . All particles were forced to decay semi-leptonically. The p_t-weighted distributions were then obtained as described in Section 12.3.

The rapidity and p_t distributions of the parent particles and of their decay electrons are shown in Fig. 12.9 and Fig. 12.10 for B and D mesons, respectively. The upper row shows the parent particle distributions, the lower one the distributions of their decay electron. The rapidity interval of the primary particles was restricted to $-4 < y < 4$ in these projections. The solid lines correspond to the input distributions. The dashed lines show the same distributions in the TRD acceptance. The rapidity distributions of accepted B and D mesons are Gaussian-like with a $\sigma = 0.93$ for B and $\sigma = 0.89$ for D mesons. The accepted electrons from B decays have a $< p_t >= 2.54$ GeV/c , those from D decays yield a $< p_t >= 1.32$ GeV/c . The B and D differential acceptance as function of rapidity and p_t are shown in Fig. 12.11 and Fig. 12.12 respectively. At mid-rapidity the acceptance varies between 50% and 90%.

The finite lifetime of B and D mesons, $c\tau = 496$ μm and $c\tau = 315$ μm , respectively, was used to develop a strategy to separate electrons coming from B and D decays from those originating from other (promptly decaying) particles ($\pi^0, \rho, \omega, \phi, J/\psi$) as described in the TRD TP [2]. It is based on the selection of non-primary high p_t electrons by optimizing selection criteria based on their transverse distance of closest approach to the primary vertex, d_0, and on their p_t. Complete simulation of the impact parameter resolution will be obtained only after optimization of the global tracking, matching the TRD tracks to those in the TPC and ITS. For the present geometrical studies d_0 is calculated from the nominal momentum of the decay lepton and the positions of the primary and secondary vertices without taking into account any detector resolutions. The effect of the detector resolution was investigated in the TRD TP [2].

Figures 12.13 and 12.14 show the rapidity and transverse momentum distributions of accepted B mesons under different selection criteria. The solid line shows the distributions of accepted B's with no further cuts on the d_0 and p_t of the decay electron, the other lines the same distributions for $d_0 > 200$ μm and $p_t > 0.5$ GeV/c (dashed line), $p_t > 1$ GeV/c (dotted line) and $p_t > 3$ GeV/c (dash-dotted line). The integrated acceptances are summarized in Table 12.3. Those cuts need to be optimized on the basis of the global tracking results. However, in Refs. [26, 27] it was shown that while a $d_0 > 100$ μm might be optimistic, a 200 μm cut should be safe. It was also shown in the TRD TP [2] that p_t cuts significantly reduce the background due to the primary particle multiplicity.

Similarly, Fig. 12.15 and Fig. 12.16 show the same distributions for D mesons, and the integrated acceptances are summarized in Table 12.3. The d_0 and p_t cuts make a stronger effect on the D acceptance.

Table 12.3: Integrated acceptance for B and D mesons in the rapidity range $|y| < 4.0$ without and with the $d_0 > 200\mu$m and p_t cuts on the decay electron accepted in the TRD.

parent particle	d_0 cut	accept $p_t > 0$	accept $p_t > 0.5$	accept $p_t > 1$	accept $p_t > 3$
B	no cut	17.3 %	12.3 %	8.1 %	1.5 %
B	$d_0 > 200\mu$m	7.4 %	3.7 %	1.9 %	0.17 %
D	no cut	15.0 %	5.9 %	2.1 %	0.055 %
D	$d_0 > 200\mu$m	5.5 %	4.4 %	0.05 %	-

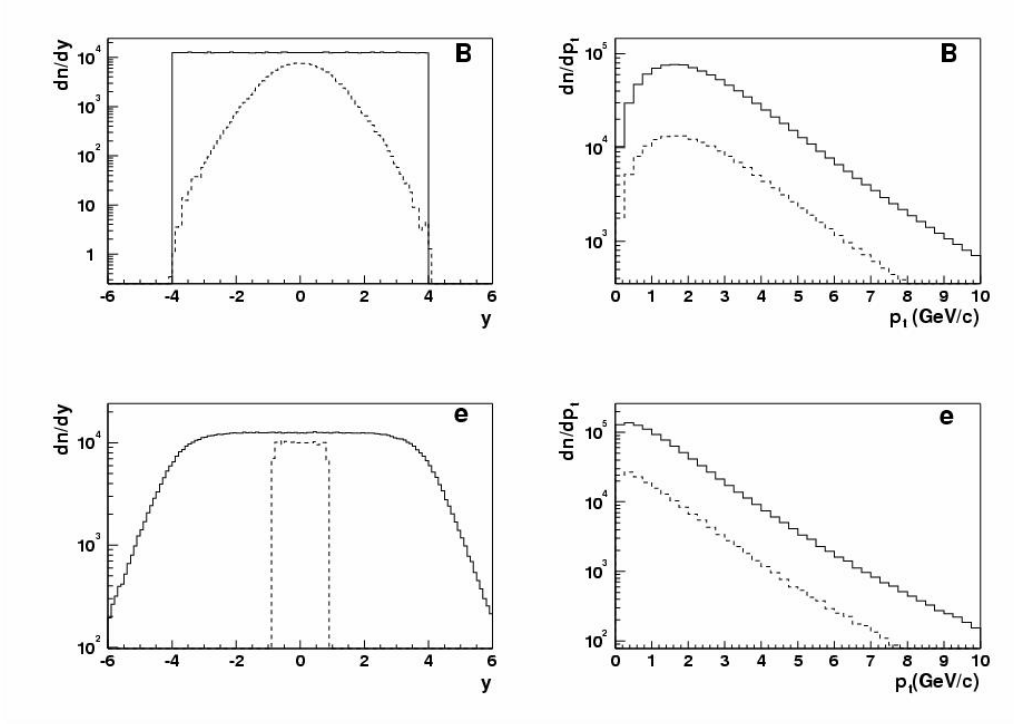

Figure 12.9: Rapidity and p_t distributions of B mesons top row, and its decay electron bottom row; full line, input distributions and dashed line accepted in TRD.

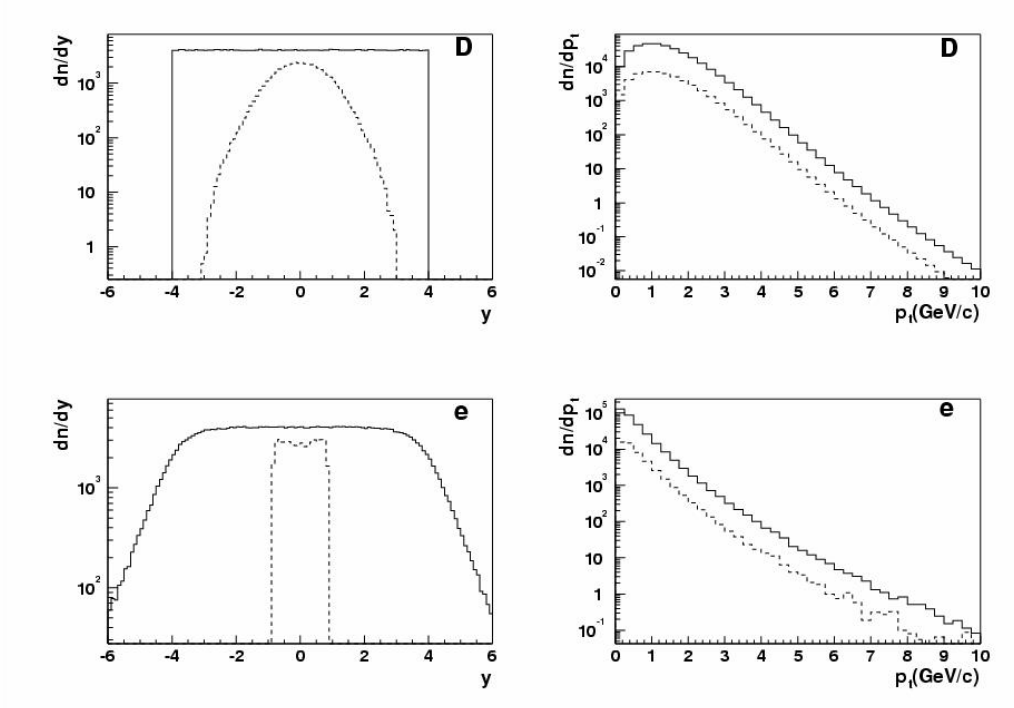

Figure 12.10: Rapidity and p_t distributions of D mesons (top row), and corresponding decay electrons (bottom row); full lines depict input distributions, dashed lines are for particles accepted in TRD.

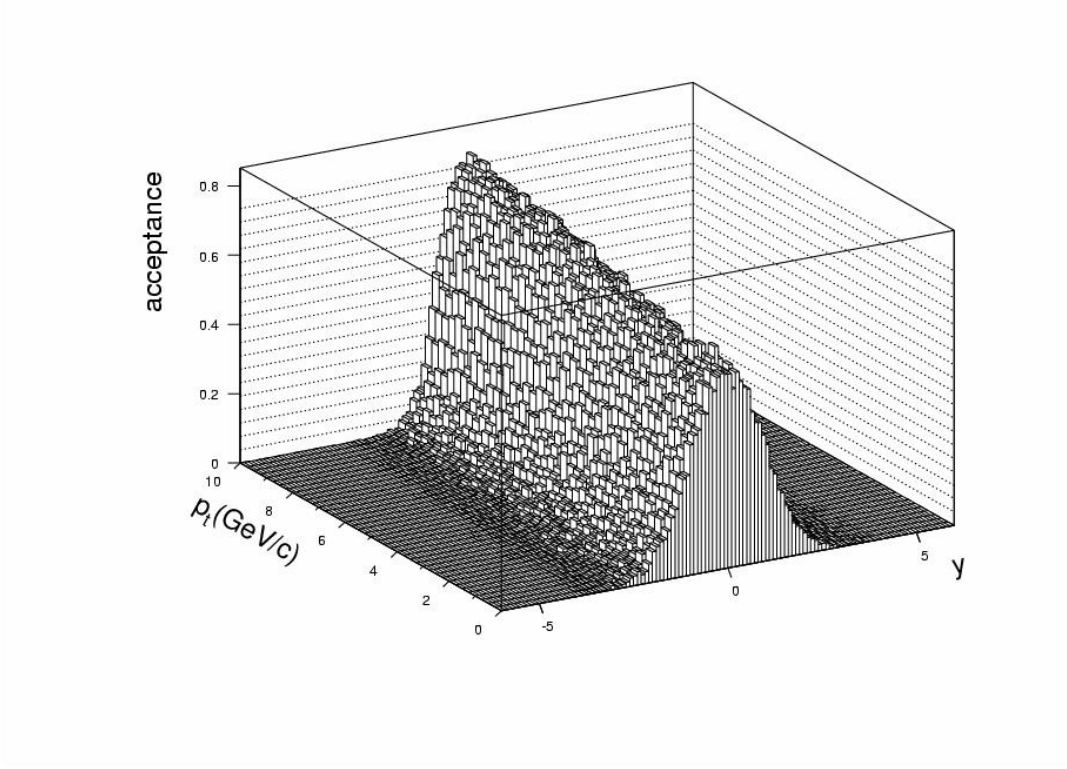

Figure 12.11: Acceptance for B mesons in the y-p_t plane.

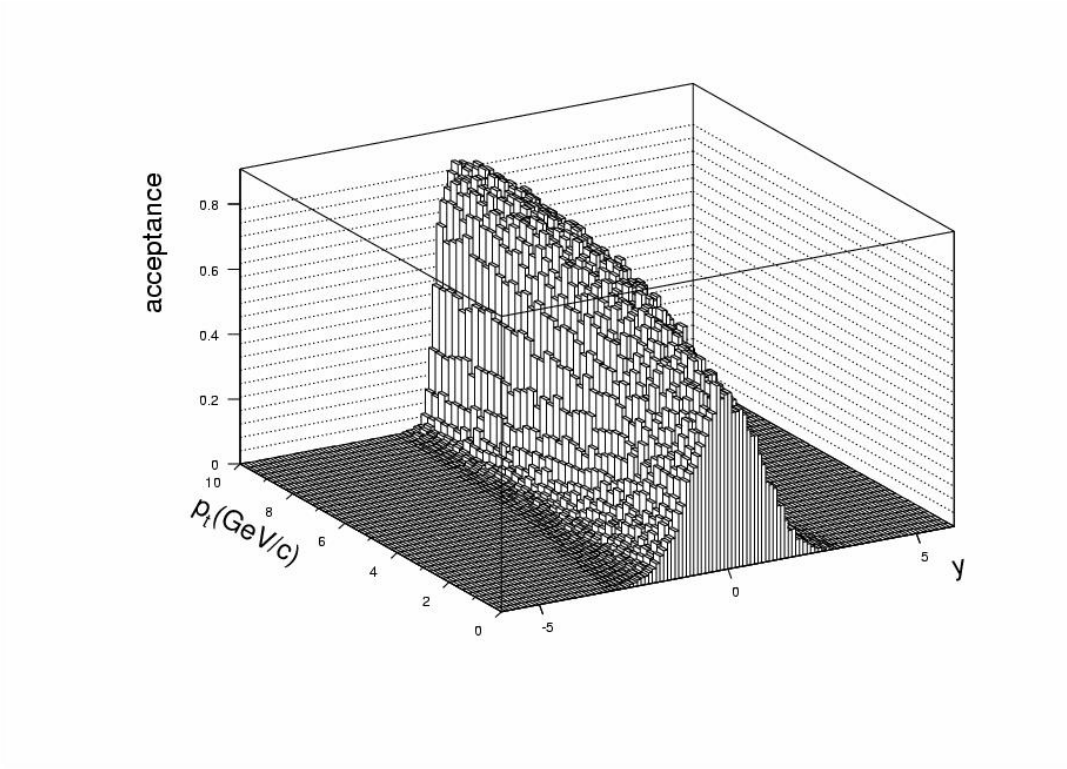

Figure 12.12: Acceptance for D mesons in the y-p_t plane.

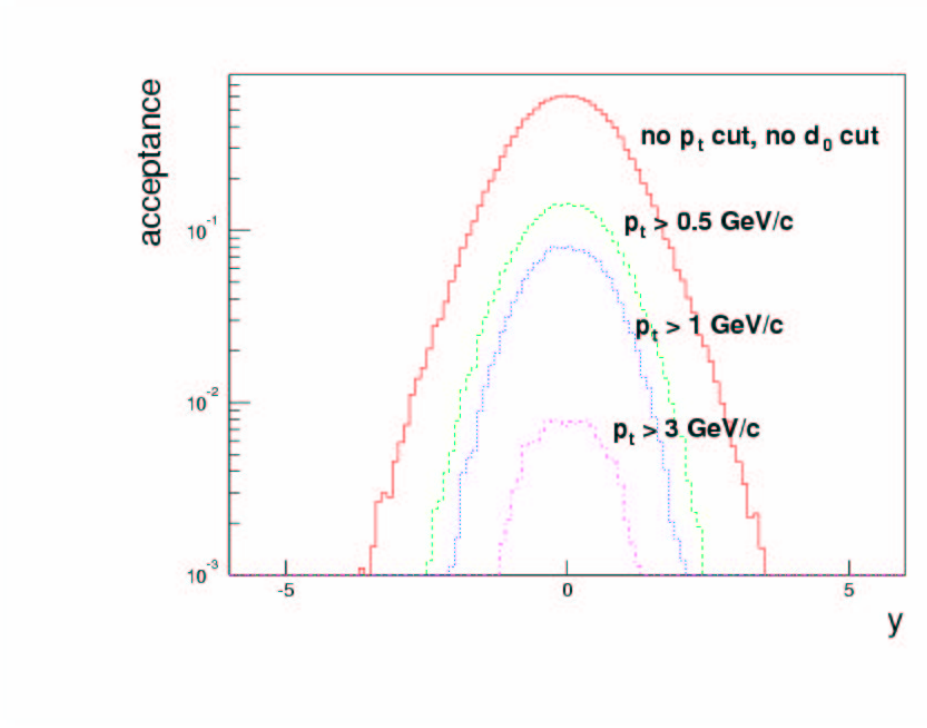

Figure 12.13: Rapidity acceptance for B mesons without cuts and for various cuts on the p_t of the decay electron. All p_t cuts contain also a cut on the d_0 variable discussed in the text.

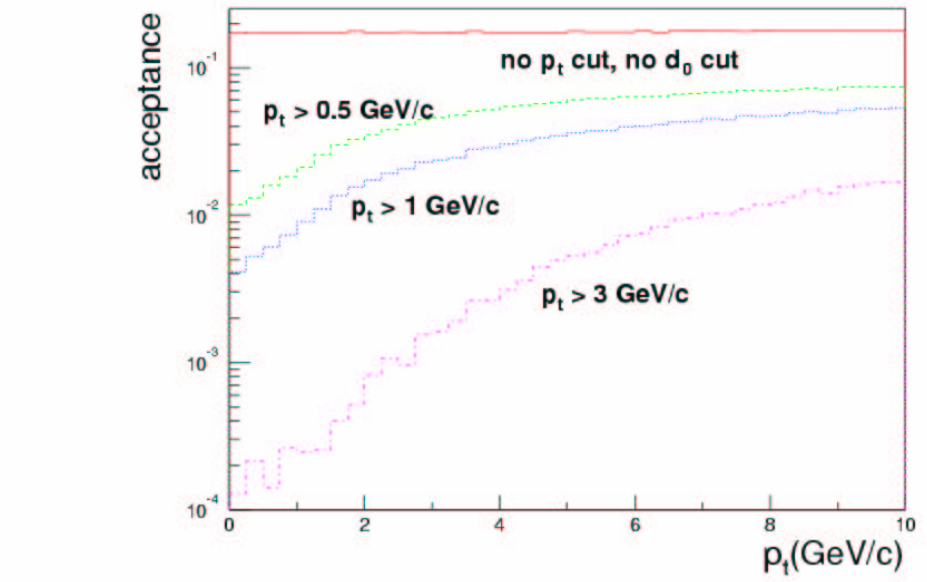

Figure 12.14: Transverse momentum acceptance for B mesons without cuts and for various cuts on the p_t of the decay electron. All p_t cuts contain also a cut on the d_0 variable discussed in the text.

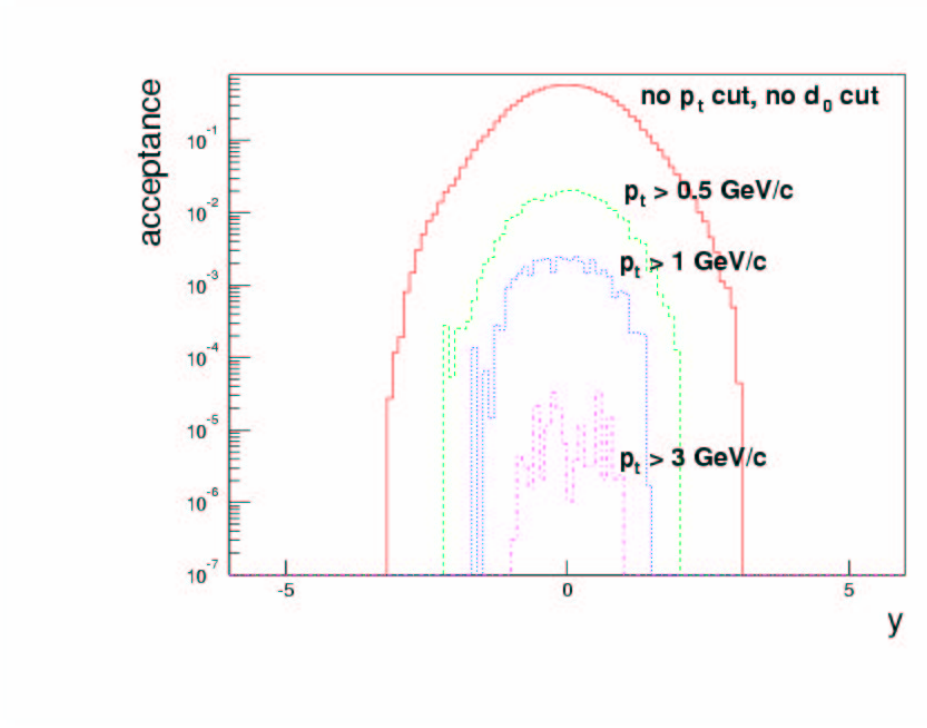

Figure 12.15: Rapidity acceptance for D mesons without cuts and for various cuts on the p_t of the decay electron. All p_t cuts contain also a cut on the d_0 variable discussed in the text.

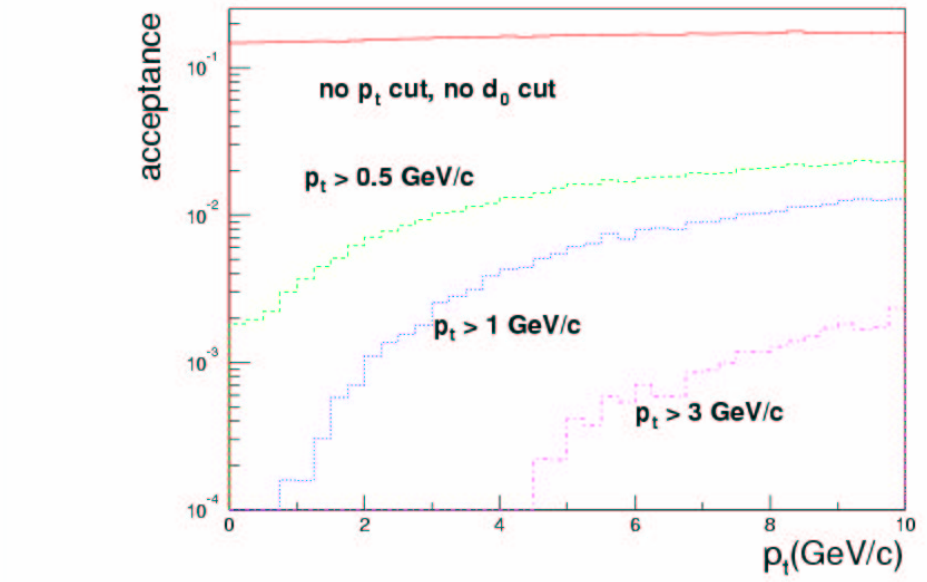

Figure 12.16: Transverse momentum acceptance for D mesons without cuts and for various cuts on the p_t of the decay electron. All p_t cuts contain also a cut on the d_0 variable discussed in the text.

12.6 TRD acceptance for different geometrical configurations

The number of detector modules that can be afforded by the Collaboration on time for the start-up of the LHC is not presently known. Therefore, a study was performed to evaluate the TRD acceptance for different geometrical configurations [25]. Different considerations were taken into account in optimizing the detector acceptance, namely the number of currently affordable stacks of detector modules, different strategies for the completion of the detector and how they would affect the overall installation planning.

The financing of the construction of the full TRD detector, consisting of 540 detector modules arranged in 90 stacks, which would cover the pseudo-rapidity range $-0.9 \leq \eta \leq 0.9$ and the full azimuth is so far not assured. The present commitments until the start-up of the LHC are sufficient to build only about half of the total number of the TRD modules. Participation of other groups that would make possible the construction of the full TRD on time for the start-up is sought but currently not guaranteed. Additional funding for the completion of the full TRD detector is expected from the funding agencies of the TRD groups; in this case the detector will be completed later than the start-up date. Therefore, at present, it cannot be ruled out that a partial TRD will be finally all that might be affordable by the Collaboration.

Those considerations lead to three possible scenarios; (a) completion of the full detector for start-up, (b) partial construction and installation of the TRD for start-up with its completion after 2 or 3 years and (c) undesirable but not excluded currently, a partial TRD only.

As discussed in Chapter 16, the TRD stacks will be assembled in supermodules which will then be inserted in the space frame. In the case that only a part of the full TRD detector would be constructed at start-up and its completion would follow at a later stage, one would have to optimise the installation procedure even at the expense of the physics performance for the first year of running. It is difficult to imagine that the supermodules would be only partialy filled and installed in the space frame at a first stage, to be taken out and completed in a later stage; this would also imply redoing all the services, alignment and calibrations.

The acceptance for the detection of the semi-leptonic decays of D and B mesons is proportional to the solid angle covered by a given TRD layout. For Υ and J/ψ this is not the case since electron pairs have to be detected in coincidence, introducing geometrical correlations. The low p_{t} primary particles decay emitting the $\mathrm{e}^{+}\mathrm{e}^{-}$ pair back to back in the laboratory frame and therefore the coverage at the opposite sides of the interaction point gives the largest yields of detected Υ. As the p_{t} of the primary particle increases, the decay kinematics focuses the electron-positron pair closer and closer and therefore a large coverage at the same side of the interaction point is optimal.

The acceptance of Υ, J/ψ, B and D mesons were calculated for three partial TRD configurations and compared to that for the full TRD detector.

The configuration called 'WING' has 10 fully filled supermodules distributed as a symmetric two-arm spectrometer with a total of 50 stacks. From the installation point of view this would be the preferred configuration for a partial TRD at a first stage which would be completed one or two years after start-up.

On the other hand, if at a certain point it becomes clear that there will not be enough funds to complete the full TRD detector, one would have to optimize the phase space coverage and distributing the available modules into complete supermodules might not be the best strategy.

The two other configurations 'SHORT' and 'SHORTASYM' consist of a compact TRD with no holes in azimuth, however, with only 3 out of 5 stacks of each supermodule being installed. Both of them have 54 stacks. The configuration 'SHORT', being centered in z around the interaction point, provides a symmetric coverage in rapidity. The 'SHORTASYM' is displaced having the two empty stacks on the same side of the supermodule. In this way the 'SHORTASYM' provides larger coverage of rapidity; however it implies an asymmetric weight distribution on the space frame. Those two configurations represent the type of solution one might choose in case it would be clear that the TRD could not be fully financed.

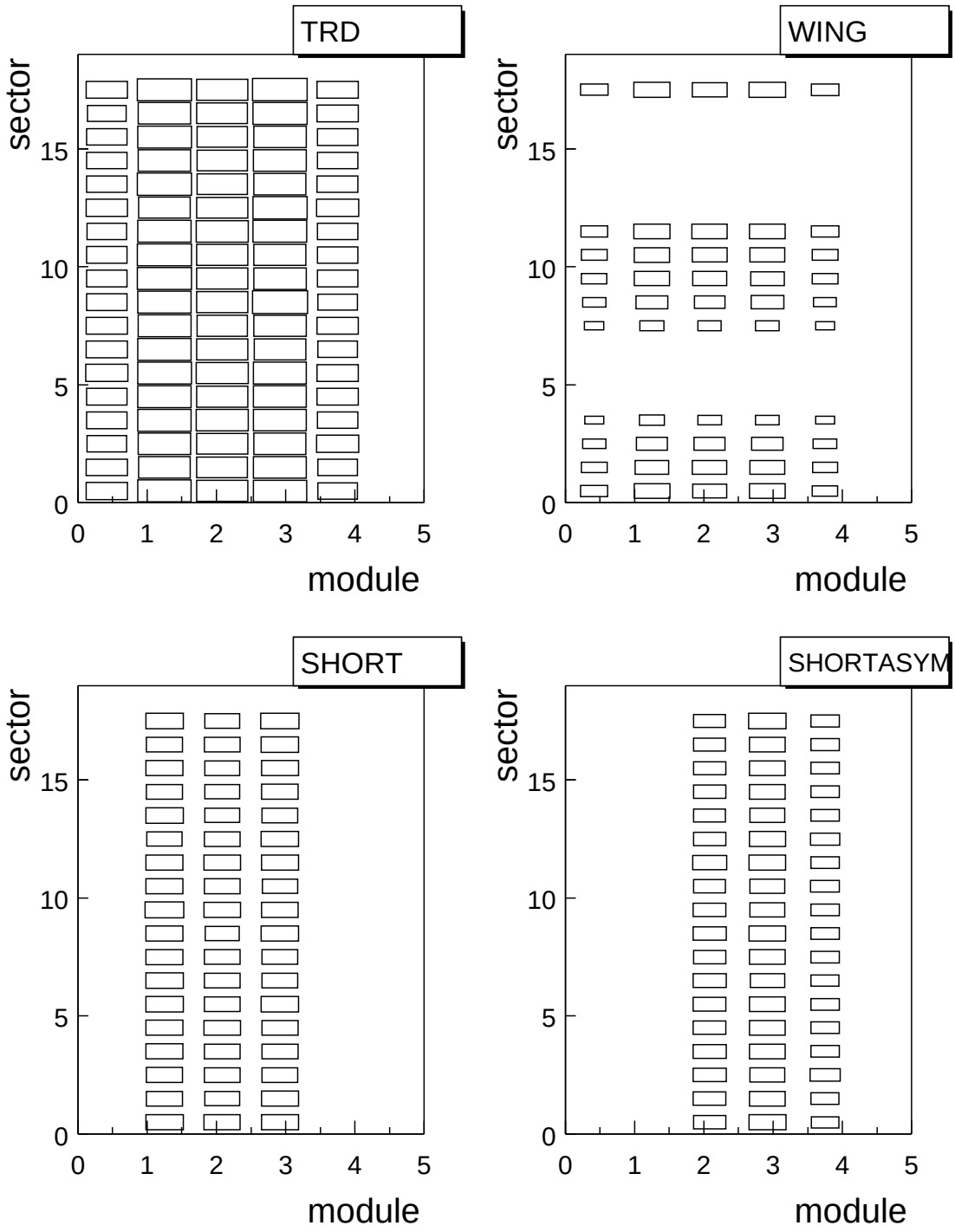

Figure 12.17: The inner layer of the TRD for the different geometries considered; the horizontal axis gives the sementation in z and the vertical in φ. Each module is represented by a rectangle. The area of each rectangle is proportional to the acceptance of the corresponding module for e^+e^- from ϒ decays. From the top left to bottom right the geometries are: 'TRD', 'WING', 'SHORT'and 'SHORTASYM'.

Figure 12.17 shows in a graphical way the ϒ acceptance for the different geometrical configurations. Figure 12.18 shows the B acceptance for the same configurations. Top row left shows the full TRD geometry (labelled "TRD") and right the 'WING' configuration. The bottom row left shows the 'SHORT'

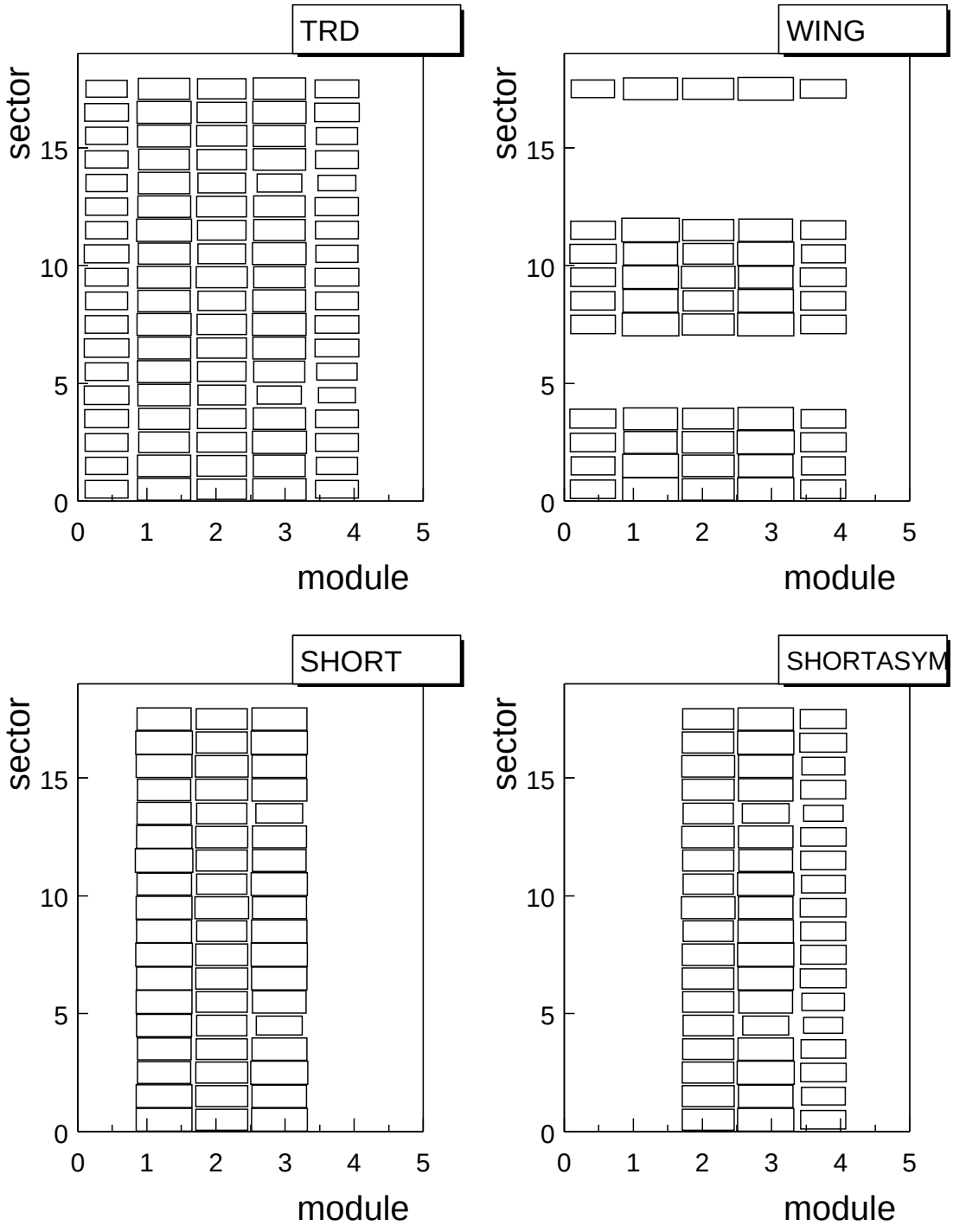

Figure 12.18: Same as Fig. 12.17 for electrons from B decays.

and right the 'SHORTASYM' configuration. Since the distribution of chambers is identical for all layers only the innermost layer for each configuration is shown with each rectangle representing a module; the horizontal axis gives the segmentation in z and the vertical that in ϕ, hence each row corresponds to a sector and represents a supermodule. Clearly visible are the holes in the TRD layout for each one of the studied configurations. The area of each module is proportional to the number of electrons from Υ or B decays, respectively, that the module accepts.

The acceptances for the three studied partial configurations, relative to the full TRD, are summarized in Table 12.4.

Table 12.4: Fractional acceptance in % of the different TRD configurations relative to the full TRD for the detection of decay electrons from Υ, J/ψ, B and D mesons.

primary particle	'WING'	'SHORT'	'SHORTASYM'
Υ	17.4	42.8	46.1
J/ψ	34.5	47.9	43.3
B	55.9	64.3	59.9
D	55.7	63.7	59.7

12.7 Background

There are several sources of background that have to be considered while reconstructing Υ and J/ψ from their e^+e^- decay detected in the TRD.

- One of them is real e^+e^- pairs originating from Dalitz decays of π^0 , η, ρ, ω, ϕ or semi-leptonic decays of B and D mesons. Their contribution as evaluated in the TRD TP [2] is shown in Fig 12.19. At large p_t this background is dominated by e^+e^- originating from semi-leptonic decays of B and D mesons as well as from Dalitz decays of π^0 .
- Another source of background from real electron or positrons, is due to γ conversions, bremsstrahlung and secondary interactions.
- A third source of background is due to charged pions misidentified as electrons by the TRD detector.

The last two sources of background were evaluated using 100 'parametrized HIJING' events as input to the simulation with all the central barrel detectors enabled. Figure 12.20 shows the p_t spectra of charged pions, electrons from conversions, bremsstrahlung and secondary interactions as well as e^+e^- from Dalitz decays of π^0 that reach the TRD detector. The e^+e^- from conversions and bremsstrahlung in the material before the TRD are an order of magnitude larger than those from π^0 Dalitz decays.

What fraction of the charged pion spectrum will contribute to the background depends on the electron identification and pion rejection capabilities that the final detector will achieve. As was shown in Chapter 11 the fraction of pions misidentified as electrons depends on the required purity of the electron sample and on the multiplicity of the event. Also the global tracking will accept only a fraction of electrons and 'electron like' particles, namely those having a good χ^2 for being primary particles and having a good likelihood of being electrons according to the dE/dx in the ITS, TPC and TRD and according to the transition radiation in the TRD.

12.8 Summary

The main conclusions from the studies presented here are:

1. Acceptances for Υ and high p_t J/ψ measurements need the full TRD.
2. The mass resolution for Υ measurements is of the order of 1% if the magnetic field of the L3 magnet is $B = 0.4$ T or larger.
3. The main background sources in the electron channel are misidentified pions and conversions.

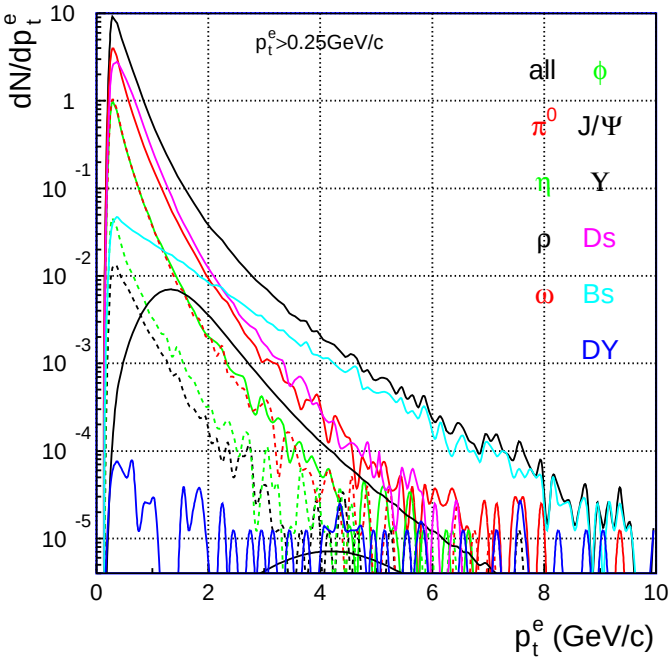

Figure 12.19: Transverse momentum spectrum of single electrons in the TRD acceptance from decays of primary particles.

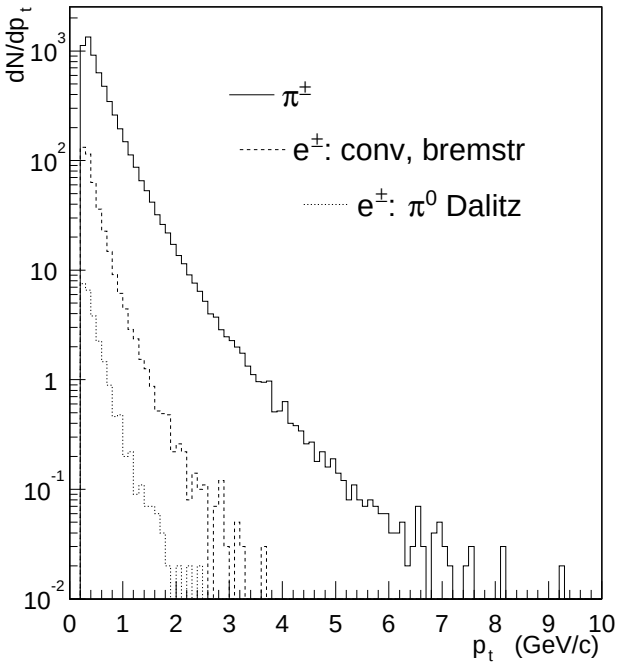

Figure 12.20: Transverse momentum spectrum of charged pions (solid line), e^+e^- from conversions, bremsstrahlung and secondary interactions (dashed line) and e^+e^- from π^0 Dalitz decays (dotted line) in the TRD detector.

4. The measurement of D and B mesons via their semi-leptonic decays can be performed with high efficiency for p_{t} cuts of the order of 1 GeV/c and higher.